Convergence of Conduction Bands as a Means of Enhancing Thermoelectric Performance of n-Type $Mg_{2}Si_{1-x}Sn_{x}$ Solid Solutions

Wei Liu, Xiaojian Tan, Kang Yin, Huijun Liu, Xinfeng Tang, Jing Shi, Qingjie Zhang, and Ctirad Uher

Phys. Rev. Lett. **108**, 166601 — Published 18 April 2012

DOI: 10.1103/PhysRevLett.108.166601

Convergence of Conduction Bands as a means of Enhancing Thermoelectric Performance of n-type $Mg_2Si_{1-x}Sn_x$ Solid Solutions

Wei Liu, [†] Xiaojian Tan, [‡] Kang Yin, [†] Huijun Liu, [‡] Xinfeng Tang, [†,*] Jin Shi, [‡] Qingjie Zhang [†] and Ctirad Uher [§,*]

[†] State Key Laboratory of Advanced Technology for Materials Synthesis and Processing, Wuhan University of Technology, Wuhan 430070, China

[‡] Key Laboratory of Artificial Micro- and Nano-structures of Ministry of Education and School of Physics and Technology, Wuhan University, Wuhan 430072, China

[§] Department of Physics, University of Michigan, Ann Arbor, Michigan 48109, USA

[*] Correspondence should be addressed; E-mail: tangxf@whut.edu.cn and cuher@umich.edu

Abstract: Mg_2Si and Mg_2Sn are indirect band gap semiconductors with two low-lying conduction bands (the lower mass and higher mass bands) that have their respective band edges reversed in the two compounds. Consequently, for some composition x, $Mg_2Si_{1-x}Sn_x$ solid solutions must display convergence in energy of the two conduction bands. Since $Mg_2Si_{1-x}Sn_x$ solid solutions are among the most prospective of the novel thermoelectric materials, we set on exploring the influence of such band convergence (valley degeneracy) on the Seebeck coefficient and thermoelectric properties in a series of $Mg_2Si_{1-x}Sn_x$ solid solutions uniformly doped with Sb. Transport measurements carried out from 4 K to 800 K reveal a progressively increasing Seebeck coefficient that peaks at x = 0.7. At this concentration the thermoelectric figure of merit *ZT* reaches exceptionally large values of 1.3 near 700 K. Our first principles calculations confirm that at the Sn content x ≈ 0.7 the two conduction bands coincide in energy. We explain the high Seebeck coefficient and *ZT* values as originating from enhanced density-of-states effective mass brought about by the increased valley degeneracy as the two conduction bands crossover. We corroborate the increase in the density-of-states effective mass by measurements of the low temperature specific heat. The research suggests that striving to achieve band degeneracy by means of compositional variations is an effective strategy for enhancing thermoelectric properties of these materials.

Key words: n-type $Mg_2Si_{1-x}Sn_x$, conduction band structure, band convergence and degeneracy, thermoelectric properties.

The efficiency of thermoelectric conversion depends on the value of the dimensionless figure of merit [1,2] defined as $ZT=\alpha^2\sigma T/(\kappa_e+\kappa_{ph})$, where α is the Seebeck coefficient, σ is the electrical conductivity, T is the absolute temperature, and κ_e and κ_{ph} are electronic and lattice contributions to the thermal conductivity. A vast majority of recent efforts to improve TE performance focused on reducing the lattice thermal conductivity by enhancing phonon scattering by processes such as alloying, extreme anharmonicity or introducing fine nanoinclusions into the bulk matrix [3-10]. In some instances, the lattice thermal conductivity was successfully reduced to near the amorphous limit [11]. Clearly, any further optimization of TE properties will require an enhancement of the numerator of the figure of merit ($\alpha^2\sigma$) called the power factor and, specifically, the Seebeck coefficient while maintaining high electrical conductivity.

The Seebeck coefficient α is related to the logarithmic derivative of electrical conductivity as [12]

$$\alpha=\frac{\pi^2}{3}\left(\frac{k_B^2T}{q}\right)\left(\frac{d\ln\sigma(E)}{dE}\right)_{E=E_F}=\frac{\pi^2}{3}\left(\frac{k_B^2T}{q}\right)\left[\frac{1}{n}\frac{dn(E)}{dE}+\frac{1}{\mu}\frac{d\mu(E)}{dE}\right]_{E=E_F} \quad (1)$$

where $n(E)$ and $\mu(E)$ are energy dependent carrier density and mobility, respectively. Large Seebeck coefficient can thus be achieved by (a) increasing the density of states near the Fermi level by, e.g., forming localized resonant states through doping [13] or by increasing band degeneracy via temperature assisted band convergence [14], (b) by increasing the energy dependence of $\mu(E)$ using energy filtering [15,16].

$Mg_2Si_{1-x}Sn_x$ solid solutions are promising candidates for mid-temperature range energy conversion [17-26] because their constituting elements are abundant, inexpensive, environmentally harmless, and do not contain scarce and expensive Te nor toxic Pb. Zaitsev et al. [17,18] pointed out the presence of both heavy and light bands in the energy spectrum of the conduction band and the possibility of band convergence. Since no systematic investigations of the conduction bands merging have as yet been considered, we were intrigued by a prospect of band convergence in $Mg_2Si_{1-x}Sn_x$ and whether it can lead to exceptionally high values of the Seebeck coefficient. For that purpose, we prepared a series of single phase n-type $Mg_2Si_{1-x}Sn_x$

solid solutions ($0.2 \leq x \leq 0.8$) and measured their transport parameters over a broad range of temperatures from 4 K to 800 K. Through a systematic experimental work (see supplemental material, especially Figs. S5 and S6), we established that n-type $Mg_2Si_{1-x}Sn_x$ with different Sn contents all achieve the optimized performance when the electron density stands near $n = 1.8\times10^{20}$ cm^{-3}. We aimed at this carrier concentration by doping with Sb, see Table 1. Figure 1 plots the temperature dependence of thermoelectric properties for our n-type $Mg_2Si_{1-x}Sn_x$. Clearly, Sn content has a strong effect on the magnitude of the Seebeck coefficient, the power factor, thermal conductivity and the figure of merit. We note that for the Sn content x = 0.7, the enhancement in the Seebeck coefficient is particularly large and is maintained in the entire range of temperatures from 300 K to 800 K. Because of the smaller rate of decrease in the electrical conductivity (see supplemental information), the power factor of n-type $Mg_2Si_{1-x}Sn_x$ rises rapidly with the Sn content and peaks at x = 0.7. Low values of the total thermal conductivity and the lattice term augmented by any bipolar contribution for compositions x = 0.6 and 0.7 are the consequence of strong alloy scattering [17,18] which, together with much enhanced power factors, contribute to exceptionally high values of $ZT \sim 1.3$ for the two solid solutions. The sample with x = 0.6 reaches this value at temperatures near 750 K while the maximum for the x = 0.7 sample occurs near 700 K. The lower temperature at which ZT peaks in the case of x = 0.7 is the consequence of a somewhat reduced band gap in this solid solution [17]. Compared with the best results in the literature [Refs.18-20], samples with x = 0.6 and 0.7 have higher ZT values due mainly to the possibly varying phase structure caused by the different synthesis process and the robust Seebeck coefficient supported by a larger valley degeneracy arising from the band convergence, as we discuss in the following paragraphs.

In iso-electronic solid solutions the dominant effect on the mean-free path of electrons are phonons and point defects. This is clearly seen in Fig. S7 where the lowest mobilities are observed near x = 0.5 and the temperature dependence at higher temperatures reflects the dominance of acoustic phonon scattering [27-29]. Thus, referring to the Mott equation (Eq.1), the observed enhancement in the Seebeck coefficient and the figure of merit of our n-type $Mg_2Si_{1-x}Sn_x$ is not due to gains in the carrier mobility and $d\mu(E)/dE$ but, rather, a result of the enhanced localized density of states at the Fermi level.

To substantiate this point, we carried out first principles calculations of the band

structure of $Mg_2Si_{1-x}Sn_x$ using a plane-wave pseudopotential formalism [30,31] based on the density functional theory. The details are given in supplemental information.

Figure 2 shows the relative motion of the highest valence band and the positions of the two lowest conduction bands (the light C_L and the heavy C_H bands separated in energy by ΔE) as the content of Sn increases from x = 0 to x = 1. While the C_H band moves monotonously down in energy with the increasing x, the C_L band moves first down and, above x = 0.3, up in energy. The two bands thus converge and the theory predicts a crossover at the Sn content of x = 0.65 ~ 0.70. This is precisely where we observe the highest values of the Seebeck coefficient and exceptional values of the figure of merit.

In an n-type semiconductor consisting of two conduction bands, the total electronic conductivity (σ_{total}) and the Seebeck coefficient (α_{total}) are given as

$$\sigma_{total}=\sigma_1+\sigma_2 \tag{2}$$

$$\alpha_{total}=(\sigma_1\alpha_1+\sigma_2\alpha_2)/\sigma_{total} \tag{3}$$

Here σ_1 and σ_2 are the respective electrical conductivity contributions from each conduction band and α_1 and α_2 are the corresponding Seebeck coefficients. Thus, the total Seebeck coefficient of $Mg_2Si_{1-x}Sn_x$ is a weighted average of the Seebeck coefficients of the individual C_H and C_L bands [14,32]. Apparently, as ΔE decreases, the heavy band C_H provides a progressively increasing contribution to the electrical properties which results in the larger effective mass and the absolute value of the Seebeck coefficient [33]. When the energy difference between C_H and C_L is less than 2 k_BT, the two conduction bands become effectively degenerate and the number of symmetrically nonequivalent pockets of electrons (valleys) N_v increases. Since the overall density-of-states effective mass is related to the valley degeneracy as $m^*=N_v^{2/3}m_s^*$, where m_s^* stands for the density-of-states effective mass of a single carrier pocket, merging of the bands enhances the carrier mass and thus the Seebeck coefficient, all without any adverse effect on the carrier mobility [14,32,34]. Moreover, since $PF_{opt}\propto\mu(m^*/m_0)^{3/2}$, exceptionally high power factors are achieved. Coupled with a significantly reduced lattice thermal conductivity on account of very effective alloy scattering, the convergence of the two conduction bands in n-type $Mg_2Si_{1-x}Sn_x$ leads to exceptionally high values of the figure of merit.

Inducing band convergence falls into the realm of carrier pocket engineering, the

concept first proposed in the context of lower dimensional structures [5,35]. Recently, this strategy was used with a spectacular success [14] with bulk p-type $PbTe_{1-x}Se_x$ solid solutions where the valence band convergence was achieved by raising the temperature. In our case, the conduction band convergence in n-type $Mg_2Si_{1-x}Sn_x$ arises from a strong dependence of band edges on the content of Sn.

To confirm the gain in the density-of-states effective mass as the light and heavy conduction bands converge in $Mg_2Si_{1-x}Sn_x$, we measured the low temperature heat capacity C_p of several solid solutions and determined the electronic heat capacity coefficient γ in the expression $C_p=\gamma T+bT^3$, where bT^3 stands for the lattice contribution. The coefficient γ provides a direct measure of the density of states at the Fermi level $N(E_F)$ and, in turn, the effective mass [36,37]

$$\gamma=\frac{\pi^2}{3}k_B{}^2N(E_F)=1.36\times10^{-4}\times V_{mol}^{2/3}n_\gamma^{1/3}\frac{m^*}{m_0} \qquad (4)$$

Here, V_{mol} is the molar volume, n_γ the number of electrons per formula unit, m^* is the density-of-states effective mass and m_0 is the mass of an electron in vacuum. A plot of C_p/T vs. T^2 yields a straight line, see Fig.3, and the intercept with the ordinate at $T = 0$ K is the value of γ. Effective masses thus obtained are presented in Table 1. Except for the sample with x = 0.5 [38], the effective mass of carriers is enhanced as the Sn content increases. $Mg_2Si_{1-x}Sn_x$ with x = 0.6 and 0.7 possesses the heaviest carrier mass, increased by as much as 40% in comparison to the sample with x = 0.2. Again, the trend is consistent with the idea of converging bands and their crossover near x = 0.7. In the above analysis we implicitly assume rigid, temperature independent bands so that the extracted values of γ are relevant at elevated temperatures.

In summary, first principles calculations show that the heavy and light conduction bands in $Mg_2Si_{1-x}Sn_x$ solid solutions converge as the content of Sn increases and the bands crossover at x = 0.65 ~ 0.70. The resulting increased valley degeneracy leads to a significantly enhanced density-of-states effective mass which gives rise to large values of the Seebeck coefficient with no adverse effect on the carrier mobility. Enhanced density-of-states effective mass is corroborated independently by low temperature specific heat measurements. The effect is particularly striking at the Sn content x = 0.7 where the two bands merge in

energy. As a consequence, at Sn concentrations x = 0.6 and x = 0.7, the figure of merit reaches the maximum value of 1.3. The solid solution with x = 0.6 attains its peak *ZT* value close to 750 K while the sample with x = 0.7 reaches its peak performance at a lower temperature of 700 K on account of its slightly smaller band gap. The combined empirical and theoretical study supports a conclusion that "the carrier pocket engineering" is an effective approach of enhancing thermoelectric properties even in bulk materials. Band convergence stimulated by doping or alloying is thus a new promising avenue for optimizing properties of thermoelectric materials.

Acknowledgement:

We wish to acknowledge supports of the National Basic Research Program of China (Grant No. 2007CB607501), the Natural Science Foundation of China (Grant No. 51172174), the 111 Project (Grant No. B07040), the International Science & Technology Cooperation Program of China (Grant No. 2011DFB60150) and the CERC-CVC U.S.-China program supported by the U.S. Department of Energy under Award Number DE-P10000012.

References：

1. A. F. Ioffe, in *Semiconductor Thermoelements and Thermoelectric Cooling* (Infosearch, London, 1957).
2. G. H. Nolas, G. J. Sharp, and H. J. Goldsmid, *Thermoelectrics* (Springer, Berlin, 2001).
3. K. F. Hsu, *et al*., Science **303**, 818 (2004).
4. B. Poudel, *et al*., Science **320**, 634 (2008).
5. M. S. Dresselhaus, *et al*., Adv. Mater. **19**, 1043 (2007).
6. D. T. Morelli, V. Jovovic and J. P. Heremans, Phys. Rev. Lett. **101**, 035901 (2008).
7. H. Li, *et al*., Appl. Phys. Lett. **94**, 102114 (2009).
8. Y. Lan, *et al.*, Adv. Funct. Mater. **20**, 357 (2010).
9. M. G. Kanatzidis, Chem. Mater. **22**, 648 (2010).
10. X. Shi, *et al*., J. Am. Chem. Soc. **133**, 7837 (2011).
11. K. Biswas, *et al.*, Nature Chem. **3**, 160 (2011).
12. M. Cutler and N. F. Mott, Phys. Rev. **181**, 1336 (1969).
13. J. P. Heremans, *et al*., Science **321**, 554 (2008).

14. Y. Z. Pei, *et al*., Nature **473**, 66 (2011).

15. M. S. Dresselhaus, *et al*., Adv. Mater. **19**, 1043 (2007).

16. J. P. Heremans, C. M. Thrush, and D. T. Morelli, Phys. Rev. B **70**, 115334 (2004).

17. V. K. Zaitsev, *et al*., in *Thermoelectric Handbook, Macro to Nano,* ed. by D. M. Rowe (CRC Taylor & Francis, 2006), Chap. 29 and 31.

18. V. K. Zaitsev, *et al*., Phys. Rev. B **74**, 045207 (2006).

19. Y. Isoda, *et al*., in *Proceedings of the 25th International Conference on Thermoelectrics*, IEEE Catalog No. 06TH8931, p. 406 (2008).

20. Q. Zhang, *et al*., Appl. Phys. Lett. **93**, 102109 (2008).

21. W. Liu, X. F. Tang and J. Sharp, J. Phys. D: Appl. Phys. **43**, 085406 (2010).

22. Q. Zhang, *et al*., J. Phys. D: Appl. Phys. **41**,185103 (2008).

23. G. S. Nolas, D. Wang, and M. Beekman, Phys. Rev. B **76**, 235204 (2007).

24. T. Dasgupta, *et al*., Phys. Rev. B **83**, 235207 (2011).

25. H. L. Gao, *et al*., J. Mater. Chem. **21**, 5933 (2011).

26. S. K. Bux, *et al*., J. Mater. Chem. **21**,12259 (2011).

27. Q. Zhang, *et al*., Phys. Stat. Sol. (a) **205**, 1657 (2008).

28. Y. Noda, *et al*., Mater. Trans. JIM **33**, 845 (1992).

29. Y. Isoda, *et al*., in *Proceedings of the 26th International Conference on Thermoelectrics*, IEEE Catalog No. CFP07404, p. 251 (2007).

30. G. Kfesse and J. Hafner, Phys. Rev. B **47**, R558 (1993).

31. G. Kfesse and J. Furthmuller, Comp. Mater. Sci. **6**, 15 (1996).

32. Y. I. Ravich, B. A. Efimova, and I. A. Smirnov, in *Semiconducting Lead Chalcogenides* (Plenum, 1970).

33. G. J. Snyder and E. S. Toberer, Nat. Mater. **7**, 105 (2008).

34. G. A. Slack, In *CRC Handbook of Thermoelectrics*, ed. D. M. Rowe (CRC Press: Boca Raton, FL, 1995) p. 406.

35. O. Rabina, Y. Lin, and M.S. Dresselhaus, Appl. Phys. Lett. **79**, 81 (2001).

36. E.S.R. Gopal, in *Specific Heats at Low Temperatures* (Plenum Press, New York, 1966).

37. M. Ahrens, *et al*., Phys. B **393**, 239 (2007).

38. Although we have not detected any impurity phases in the sample with x = 0.5, it has been stated, e.g., in Ref. 18 that in the range of Sn content between about x = 0.4 and x = 0.6 Mg_2Si and Mg_2Sn are immiscible. Perhaps the anomalous values of γ and the effective mass for the x = 0.5 sample are reflections of this.

Table caption:

Table 1: Room temperature Seebeck coefficient and electronic properties of n-type $Mg_2Si_{1-x}Sn_x$ solid solutions.

Figure captions:

Figure 1: Temperature dependence of thermoelectric properties for n-type $Mg_2Si_{1-x}Sn_x$ solid solutions. Filled symbols in Figure 3c stand for the total thermal conductivity while the semi-filled symbols show values for the combination of lattice and bipolar contributions to the thermal conductivity.

Figure 2: Relative positions of the heavy and light conduction bands as well as the topmost valence band as a function of Sn content for $Mg_2Si_{1-x}Sn_x$ solid solutions. The red dashed line shows energy variation for the heavy conduction band C_H as the Sn content increases, while the blue dashed line and dark dashed line show motions of the light conduction band C_L and the valence band V, respectively. Solid dots colored with red, blue and black represent the calculated data for different Sn contents.

Figure 3: C_p/T vs. T^2 plots for selected n-type $Mg_2Si_{1-x}Sn_x$ solid solutions.

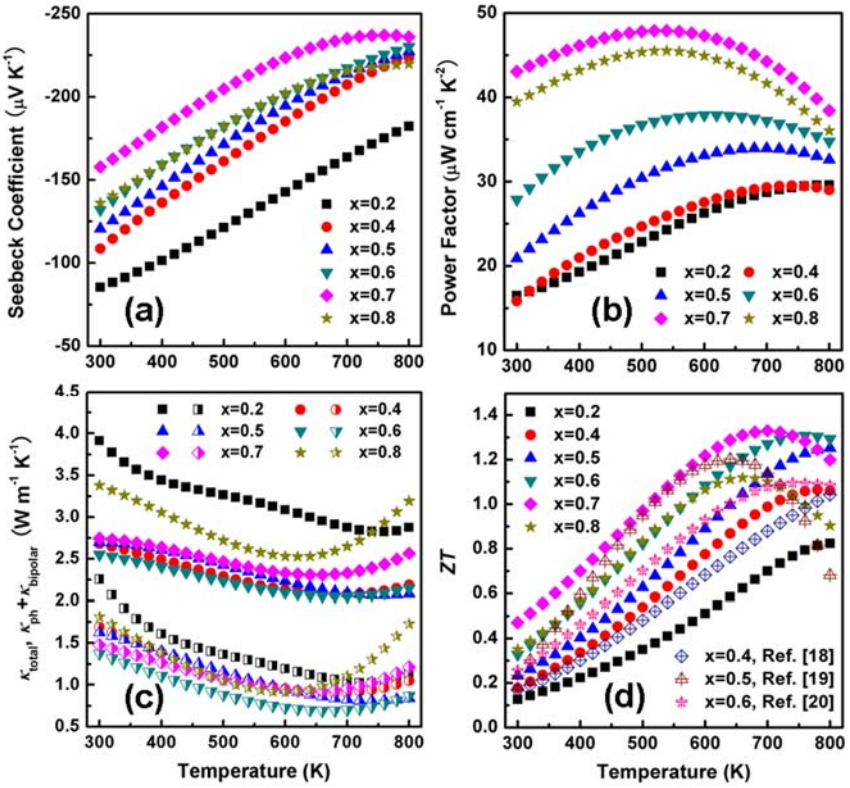

Figure 1

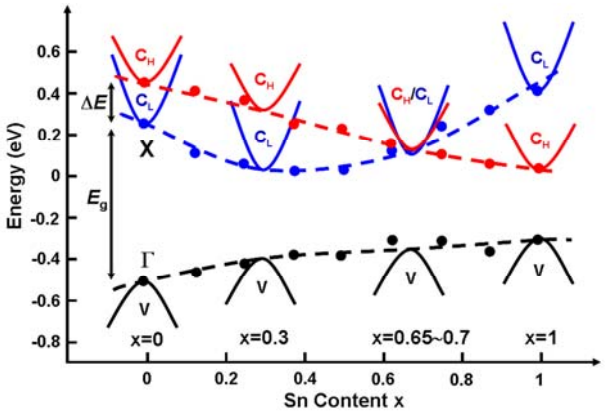

Figure 2

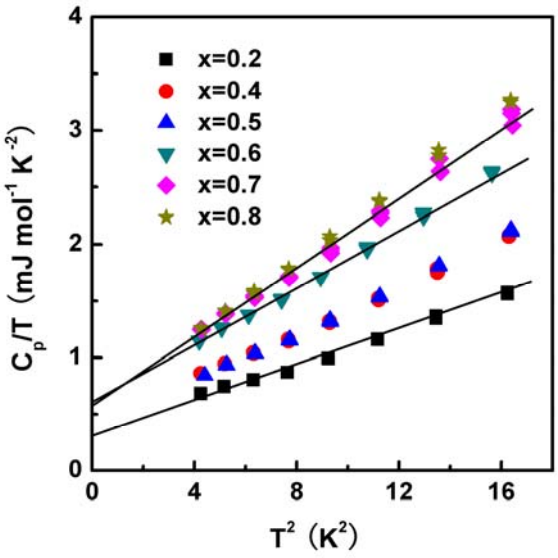

Figure 3

Table 1

Sample list	Sb doping amount y	Actual composition	α (μV K^{-1})	n (cm^{-3})	μ (cm^2 V^{-1} s^{-1})	γ (mJ mol^{-1} K^{-2})	b (μJ mol^{-1} K^{-4})	m^*/m_0	θ_D (K)
x=0.2	0.01	$Mg_{2.08}Si_{0.77}Sn_{0.22}Sb_{0.007}$	-85	1.7×10^{20}	77.2	0.33	75	0.93	294
x=0.4	0.01	$Mg_{2.11}Si_{0.58}Sn_{0.41}Sb_{0.006}$	-108	1.8×10^{20}	49.0	0.41	100	1.07	268
x=0.5	0.01	$Mg_{2.11}Si_{0.52}Sn_{0.48}Sb_{0.006}$	-121	1.9×10^{20}	47.5	0.36	107	0.90	262
x=0.6	0.015	$Mg_{2.14}Si_{0.39}Sn_{0.60}Sb_{0.009}$	-132	1.7×10^{20}	56	0.58	129	1.51	247
x=0.7	0.01	$Mg_{2.15}Si_{0.28}Sn_{0.71}Sb_{0.006}$	-158	1.7×10^{20}	64	0.55	155	1.41	232
x=0.8	0.015	$Mg_{2.06}Si_{0.18}Sn_{0.81}Sb_{0.012}$	-136	1.8×10^{20}	69.4	0.53	166	1.26	226